

## Physics of multiscale convection in Earth's mantle: Evolution of sublithospheric convection

Jun Korenaga<sup>1</sup>

Department of Earth and Planetary Science, University of California, Berkeley, California, USA

Thomas H. Jordan

Department of Earth Sciences, University of Southern California, Los Angeles, California, USA

Received 20 February 2003; revised 21 September 2003; accepted 7 October 2003; published 14 January 2004.

[1] We investigate the physics of multiscale convection in Earth's mantle, characterized by the coexistence of large-scale mantle circulation associated with plate tectonics and small-scale sublithospheric convection. In part 2 of our study, the temporal and spatial evolution of sublithospheric convection is studied using two-dimensional whole mantle convection models with temperature- and depth-dependent viscosity and an endothermic phase transition. Scaling laws for the breakdown of layered convection as well as the strength of convection are derived as a function of viscosity layering, the phase buoyancy parameter, and the thermal Rayleigh number. Our results suggest that layered convection in the upper mantle is maintained only for a couple of overturns, with plausible mantle values. Furthermore, scaling laws for the onset of convection, the stable Richter rolls, and the breakdown of layered convection are all combined to delineate possible dynamic regimes beneath evolving lithosphere. Beneath long-lived plates, the development of longitudinal convection rolls is suggested to be likely in the upper mantle, as well as its subsequent breakdown to whole mantle-scale convection. This evolutionary path is suggested to be consistent with the seismic structure of the Pacific upper mantle. *INDEX TERMS*: 3040

Marine Geology and Geophysics: Plate tectonics (8150, 8155, 8157, 8158); 8120 Tectonophysics: Dynamics of lithosphere and mantle—general; 8121 Tectonophysics: Dynamics, convection currents and mantle plumes; 8180 Tectonophysics: Tomography; *KEYWORDS*: convection, upper mantle, scaling laws

**Citation:** Korenaga, J., and T. H. Jordan (2004), Physics of multiscale convection in Earth's mantle: Evolution of sublithospheric convection, *J. Geophys. Res.*, 109, B01405, doi:10.1029/2003JB002464.

### 1. Introduction

[2] In plate tectonics on the Earth, the mantle continuously comes up to the surface beneath mid-ocean ridges and then moves laterally to subduction zones. The top boundary layer of this mantle circulation is called oceanic lithosphere, whose evolution holds a key to understand the physics of multiscale convection in Earth's mantle. After oceanic lithosphere is created at a divergent plate boundary, its subsequent thermal evolution can be modeled (approximately) as instantaneous surface cooling of a uniformly hot fluid [e.g., *Turcotte and Schubert*, 1982]. The surface cooling places the upper portion of oceanic mantle into a gravitationally unstable mode; cooler and thus denser mantle continuously grows above hotter and more buoyant mantle. Eventually, therefore, oceanic lithosphere becomes convectively unstable, leading to the generation of small-scale convection within oceanic asthenosphere [e.g., *Parsons and McKenzie*, 1978; *Buck and Parmentier*,

1986; *Davaille and Jaupart*, 1994; *Korenaga and Jordan*, 2003a]. Interaction with large-scale shear associated with plate motion tends to organize the planform of small-scale convection, creating longitudinal convection rolls, or Richter rolls [e.g., *Richter and Parsons*, 1975].

[3] For the past three decades, a number of theoretical studies have been done on small-scale convection [e.g., *Richter*, 1973a; *Yuen et al.*, 1981; *Fleitout and Yuen*, 1984; *Davies*, 1988; *Dumoulin et al.*, 1999; *Solomatov and Moresi*, 2000]. Previous studies on small-scale convection, explicitly or implicitly, assumed layered convection, i.e., convective motion is assumed to be confined to the upper mantle. Though a viscosity jump and an endothermic phase transition may temporarily hamper material flux through the 660 km discontinuity, it remains uncertain how valid it is to assume locally layered convection beneath oceanic lithosphere. To better understand the spatial scale of sublithospheric convection, its dynamics needs to be investigated in the framework of a whole mantle convection system.

[4] Assessing such a fundamental assumption is important for building a solid knowledge base regarding sublithospheric convection. Given recent advance in high-resolution upper mantle tomography, which indicates the presence of small-scale convection beneath the Pacific plate [e.g., *Katzman et al.*, 1998], it is urgent for us to be able to

<sup>1</sup>Now at Department of Geology and Geophysics, Yale University, New Haven, Connecticut, USA.

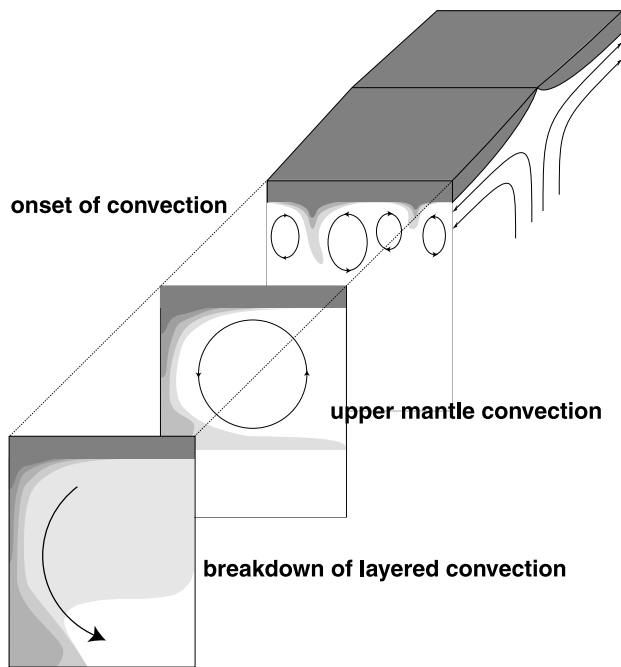


**Figure 1.** Schematic diagram of possible evolution of sublithospheric convection in oceanic mantle [after *Korenaga and Jordan, 2003a*].

predict theoretically the dynamic state of oceanic upper mantle. Such capability will with no doubt facilitate productive feedback between theory and observation. Given uncertainties regarding the physical and rheological properties of the mantle, obtaining a scaling law that can handle a wide range of parameters is essential. The purpose of this paper is, therefore, to establish scaling laws for the dynamics of a whole mantle system that exhibits both large-scale mantle circulation and small-scale convection, on the basis of a large number of 2-D numerical calculations.

[5] This paper focuses on the potential evolution of sublithospheric, so-called “small-scale” convection (Figure 1). Note that the very first phase, i.e., the onset of convection, has already been studied by *Korenaga and Jordan* [2003a]. The temporal variation of the spatial scale of sublithospheric convection is studied by 2-D convection models with temperature- and depth-dependent viscosity and an endothermic phase transition. The concept of morphological similarity is introduced here. A scaling law for the breakdown of layered convection to whole mantle convection is derived for a transient cooling problem with a range of viscosity layering and phase boundary buoyancy. Finally, combining with other scaling laws for sublithospheric convection derived in previous studies, we discuss possible dynamic regimes expected beneath oceanic plates.

## 2. Spatial Evolution of Sublithospheric Convection

[6] The spatial scale of sublithospheric convection has long been assumed to be small compared to global mantle circulation (hence sublithospheric convection and small-

scale convection are often used interchangeably). This is equivalent to assuming that sublithospheric convection is confined in the upper mantle, but how valid is this assumption? In other words, can the mantle be layered for sublithospheric convection? Though there has been extensive discussion on the possibility of layered mantle convection based on numerical modeling [e.g., *Christensen and Yuen, 1984; Machetel and Weber, 1991; Tackley et al., 1993; Puster and Jordan, 1997*], its focus has been mostly on global mantle circulation, and much less attention has been paid for the layering of sublithospheric convection. There are at least two potential mechanisms in favor of layering: depth-dependent viscosity and endothermic phase transition. Geophysical observations suggest that the lower mantle is probably  $\sim 30$  times more viscous than the upper mantle [e.g., *Hager et al., 1985; Forte and Mitrovica, 1996; Simons and Hager, 1997*]. Viscosity layering, of course, does not completely prevent cold downwelling from the base of lithosphere to sink into the lower mantle. It simply increases the timescale for penetration, which may result in the temporary layering of sublithospheric convection.

[7] An endothermic phase transition between  $\gamma$ -spinel and perovskite + magnesiowüstite that occurs at around 660 km depth [e.g., *Ito et al., 1990*], on the other hand, provides positive buoyancy due to the deformation of the phase boundary, which may partially cancel the negative thermal buoyancy. Whole mantle convection models have consistently demonstrated that a reasonable value of the Clapeyron slope (i.e.,  $-2$  to  $-3$  MPa  $K^{-1}$ ) leads to intermittent layered convection [e.g., *Machetel and Weber, 1991; Tackley et al., 1993; Honda et al., 1993; Solheim and Peltier, 1994*], except at very high Rayleigh numbers, with which complete layering is possible [e.g., *Yuen et al., 1994*]. The strength of a phase boundary in stationary state convection is the main interest of these convection studies. Previous studies on the relation between transient convection and phase change dynamics have been limited mostly to the interaction of an upwelling plume with an endothermic phase boundary [e.g., *Nakakuki et al., 1994; Schubert et al., 1995; Marquart et al., 2000*]. Nonetheless, several scaling laws have been derived to understand the phase change dynamics observed in these convection models [e.g., *Bercovici et al., 1993; Solheim and Peltier, 1994; Tackley, 1995*], and basic physical ideas behind them are quite useful for our problem.

[8] A key to understand the strength of a phase boundary with regard to convective stirring lies in the nature of a counter flow field caused by phase boundary deflection. The strength of such flow depends on the characteristic wavelength of the deflection; longer horizontal wavelength results in counter flow with a correspondingly larger vertical extent, and because viscous dissipation is proportional to the volume of a convective domain, an energetics argument requires the resultant flow to be weaker. Thus, whereas a large-scale thermal anomaly can easily penetrate an endothermic phase boundary, a small-scale anomaly may feel it as a significant barrier. *Tackley* [1995] demonstrated this by solving simple Stokes flow models. We note that this dependence on wavelength of phase boundary dynamics cannot be obtained by considering local buoyancy balance alone.

[9] This balance between ‘volume Stokes flow’ driven by thermal buoyancy and ‘boundary Stokes flow’ by phase transition buoyancy is also sensitive to finite domain effects

(i.e., distance to a phase boundary from the upper and lower mechanical boundaries) as well as detailed flow structure [Tackley, 1995]. Owing to the dynamic nature of the problem, it is difficult to apply a conventional stability analysis to derive conditions for layered convection [cf. Butler and Peltier, 1997]. This difficulty is similar in nature to that already known for the onset of convection [e.g., Howard, 1966; Korenaga and Jordan, 2003a]. We thus need to derive scaling laws by means of time-dependent numerical simulations, with a wide range of viscosity layering and phase transition parameters.

### 3. Numerical Formulation

[10] The nondimensionalized governing equations for thermal convection of an incompressible fluid with phase transition buoyancy are Conservation of mass

$$\nabla \cdot \mathbf{u}^* = 0, \quad (1)$$

Conservation of momentum

$$-\nabla P^* + \nabla \cdot [\mu^*(\nabla \mathbf{u}^* + \nabla \mathbf{u}^{*\top})] + Ra_2 T^* \mathbf{e}_z - Rb_2 \Gamma \mathbf{e}_z = 0, \quad (2)$$

Conservation of energy

$$\frac{\partial T^*}{\partial t^*} + \mathbf{u}^* \cdot \nabla T^* = \nabla^2 T^*, \quad (3)$$

where  $\mathbf{u}^*$ ,  $\mu^*$ ,  $P^*$ ,  $T^*$ , and  $t^*$  denote velocity, viscosity, pressure, temperature, and time, respectively, all of which are normalized. The spatial differential operator,  $\nabla$ , is also normalized as  $(\partial/\partial x^*, \partial/\partial y^*, \partial/\partial z^*)$ . The unit vector  $\mathbf{e}_z$  is positive upward. The spatial scale is normalized with a whole mantle height of  $D$  (2900 km), and the temporal scale is normalized with a whole mantle diffusion time of  $D^2/\kappa$ . Temperature is normalized by temperature difference between top and bottom boundaries,  $\Delta T (\equiv T_0 - T_s)$ , and viscosity is normalized by lower mantle viscosity,  $\mu_2$ .  $Ra_2$  is the thermal Rayleigh number defined as

$$Ra_2 = \frac{\alpha \rho_0 g \Delta T D^3}{\kappa \mu_2}, \quad (4)$$

where  $\alpha$  is the coefficient of thermal expansion,  $g$  is gravitational acceleration, and  $\rho_0$  is reference density at  $T = T_0$ .

[11] The boundary Rayleigh number,  $Rb_2$ , is defined as

$$Rb_2 = \frac{\Delta \rho g D^3}{\kappa \mu_2}, \quad (5)$$

where  $\Delta \rho$  is a density jump associated with the phase transition. The phase transition function,  $\Gamma$ , is defined as [e.g., Richter, 1973b; Christensen and Yuen, 1985; Zhong and Gurnis, 1994]

$$\Gamma(\Delta p^*) = \frac{1}{2} \left( 1 + \tanh \frac{\Delta p^*}{\Delta d^*} \right), \quad (6)$$

where  $\Delta p^*$  is excess pressure with reference to phase transition pressure as

$$\Delta p^* = z_r^* - z^* - \gamma^*(T^* - T_r^*). \quad (7)$$

Here  $z_r^*$  is the reference height for phase transition (independent of temperature),  $\gamma^*$  is the Clapeyron slope normalized by  $\rho_0 g D / \Delta T$ , and  $T_r^*$  is the reference temperature for phase transition. The parameter  $\Delta d^*$  is a transition length, which should be much smaller than unity but also large enough to capture phase boundary deflection with a given finite element mesh. In all of our model runs, we set  $z_r^* = 0.75$ ,  $T_r^* = 1.0$ , and  $\Delta d^* = 0.03$ . The relative importance of a phase boundary on thermal convection is controlled by the ratio of  $Rb_2/Ra_2$  as well as the Clapeyron slope, and this is summarized in the phase buoyancy parameter  $\Phi$  [e.g., Christensen and Yuen, 1985]:

$$\Phi = \gamma^* \frac{Rb_2}{Ra_2} = \frac{\gamma \Delta \rho}{\alpha \rho_0^2 g D}. \quad (8)$$

The Clapeyron slope of  $-2 \text{ MPa K}^{-1}$  with a 10% density jump and thermal expansivity of  $3 \times 10^{-5} \text{ K}^{-1}$ , for example, corresponds to  $\Phi \sim -0.07$ .

[12] The geometry of our whole mantle model is defined in Figure 2a. The upper mantle depth is denoted by  $d$ ; in our model the upper mantle simply occupies the top quarter of the model (i.e.,  $d/D = 0.25$ ). The model has a unit aspect ratio. Our main interest is, however, the evolution of upper mantle convection, for which the aspect ratio is four. We consider temperature-dependent viscosity of the Arrhenius form:

$$\mu(T, z) = \mu_0(z) \exp\left(\frac{E}{RT}\right), \quad (9)$$

where  $E$  is activation energy and  $R$  is the universal gas constant. Simple two-layer depth dependency is employed; the reference viscosity for the lower mantle,  $\mu_2$ , is higher than that for the upper mantle,  $\mu_1$ . Viscosity is normalized by  $\mu_2$ . As a measure of temperature dependency, we define the temperature derivative of logarithmic viscosity with internal temperature as [e.g., Morris and Canright, 1984]

$$\sigma = - \left. \frac{d \log \mu^*}{dT^*} \right|_{T^*=1}. \quad (10)$$

[13] The top boundary is rigid whereas the bottom boundary is free slip. Normalized temperature at the top and bottom boundaries are fixed as 0 and 1, respectively. The initial internal temperature is set to unity plus random perturbations with the maximum amplitude of  $10^{-3}$ . Our model is thus designed to investigate the temporal evolution of a mantle section with growing oceanic lithosphere. As can be seen in form of the energy equation (3), no internal heating is considered, which is justified because (1) our main interest is in the relatively early evolution of transient cooling as marked by the breakdown of layered convection; (2) Earth's upper mantle is widely believed to be depleted with heat-producing elements [e.g., Jochum et al., 1983]; and (3) the model lower mantle is hardly affected by surface

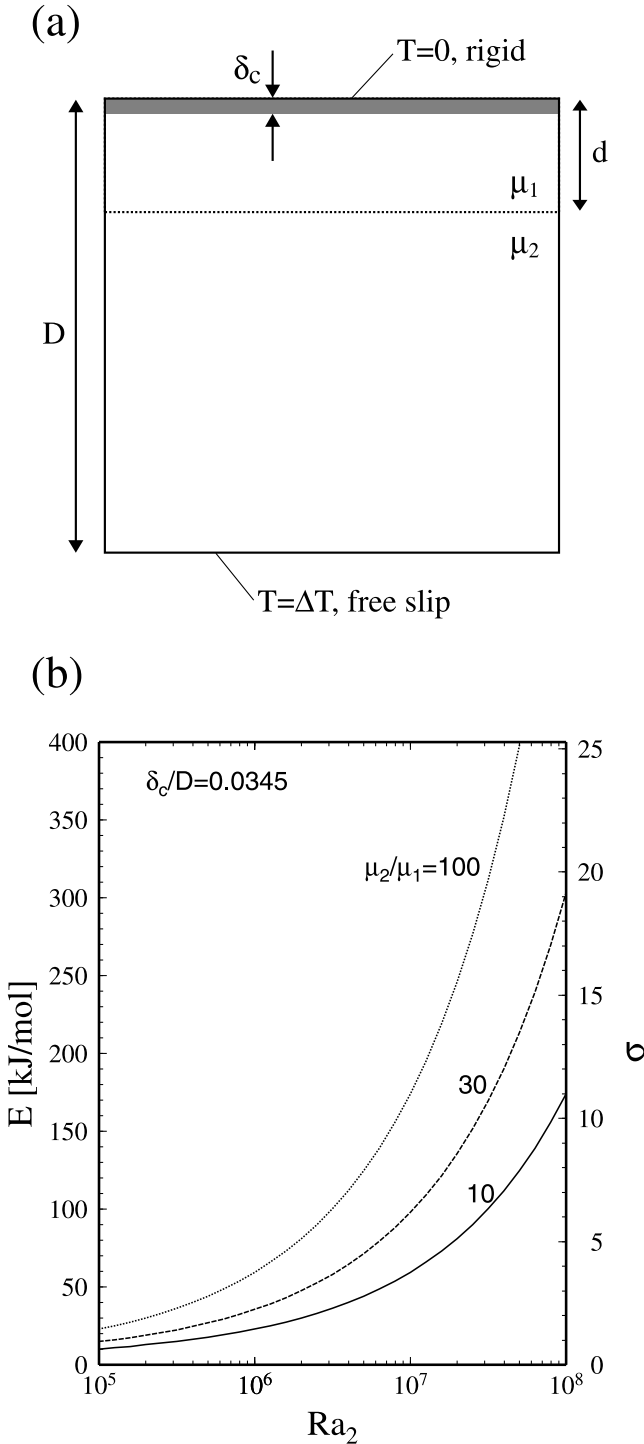


**Figure 2.** (a) Geometry of whole mantle convection model for transient cooling. (b) Activation energy as a function of  $Ra_2$  to satisfy the morphological similarity of  $\delta_c/D = 0.0345$ , based on the onset time scaling law [Korenaga and Jordan, 2003a, equation (24)] with  $Ra_c$  of 1290. Viscosity is of the Arrhenius form.

cooling during the initial layered state, so there is no need to use internal heating to maintain the hot lower mantle.

[14] In order to derive a scaling law, we need to run models with a number of different combinations of the

thermal Rayleigh number, the phase buoyancy parameter, the activation energy, and the viscosity contrast between the upper and lower mantle. A systematic approach is obviously required to handle this wealth of parameters. The accessible range of each parameter is usually constrained by available computational resources. Because testing all possible combinations is impractical, the question is how efficiently we can sample the given parameter space. Such modeling strategy is of course case-dependent. For the stability of layered sublithospheric convection, for which the finite domain effect in phase boundary dynamics is important, we believe that the concept of “morphological similarity” serves as a useful guideline. In the series of model runs with morphological similarity, the value of activation energy is chosen so that the thickness of lithosphere at the onset of convection,  $\delta_c$ , remains the same with different combinations of other parameters (Figure 2b). We choose  $\delta_c = 100$  km (i.e.,  $\delta_c^* = 0.0345$ ), so the application of our results is limited to a convection system with Earth-like lithosphere. For different combinations of  $Ra_2$  and  $\mu_2/\mu_1$ , the activation energy is calculated on the basis of our onset time scaling law [Korenaga and Jordan, 2003a, equation (24)] with the critical Rayleigh number,  $Ra_c$ , of 1290. The thickness of a rigid lid is assumed to be calculated from the origin of available buoyancy,  $\eta_0$ , as  $\delta_c = 2\eta_0\sqrt{t_c^*}$  (see [Korenaga and Jordan, 2003a] for the definition of  $\eta_0$ ). With this approach, the depth extent of small-scale convection in the upper mantle is nearly constant, and all models share the same finite domain effect on the strength of the phase boundary. By keeping morphological differences minimum, the interpretation of dynamical differences becomes more straightforward.

[15] For the purpose of discussion, it is convenient to define the local Rayleigh number for the upper mantle system as

$$Ra_{UM} = Ra_2 \frac{\mu_2}{\mu_1} \left( \frac{d - \delta_c}{D} \right)^3 \Delta T_{UM}, \quad (11)$$

where  $\Delta T_{UM}$  denotes the temperature difference driving sublithospheric convection. Using the scaling law for the onset of convection, we can estimate  $\Delta T_{UM} \sim \text{erfc}(\eta_0)$ .

[16] The breakdown of layered convection is monitored on the basis of a vertical mass flux diagnostic [e.g., Peltier and Solheim, 1992]:

$$R(z^*) = \left[ \int (w^*)^2 dx^* \right]^{\frac{1}{2}} / \int_0^1 \left[ \int (w^*)^2 dx^* \right]^{\frac{1}{2}} dz^*, \quad (12)$$

where  $w^*$  denotes the vertical component of velocity. An initial layered stage in our transient cooling problem is characterized by almost all of vertical mass flux concentrated in the upper mantle. When such a layered state is once destroyed, vertical mass flux becomes more evenly distributed throughout the mantle. We thus define the breakdown time as the first instant that satisfies

$$\int_{0.75}^{1.0} R(z^*) dz^* < 0.5, \quad (13)$$

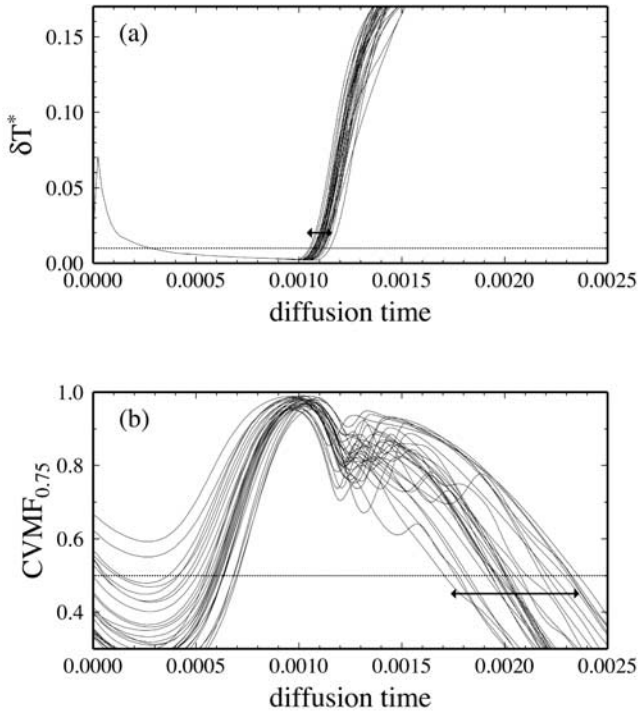


**Figure 3.** Amplified random nature of layering breakdown in relative to the onset of convection. (a) Deviation from conducting temperature profile and (b)  $\int_{0.75}^{1.0} R(z^*) dz^*$  are shown for the case of  $Ra = 10^6$ ,  $\mu_2/\mu_1 = 30$ , and  $\Phi = -0.07$  with 30 Monte Carlo realizations of initial temperature perturbations ( $\epsilon = 10^{-3}$ ). Arrows indicate the range of uncertainty based on our measurement criteria.

after the onset of convection. We will refer to the left-hand side of equation (13) as cumulative vertical mass flux (or  $\text{CVMF}_{0.75}$ ).

#### 4. Results

[17] We conducted total 90 runs, for all the possible combinations of  $Ra_2 = 3 \times 10^5, 10^6, 3 \times 10^6, 10^7$ , and  $3 \times 10^7$ ,  $\mu_2/\mu_1 = 10, 30$ , and  $100$ , and  $\Phi = 0, -0.035, -0.07, -0.105, -0.14$ , and  $-0.175$ . The corresponding range of  $Ra_{UM}$  is  $2 \times 10^4 - 3 \times 10^6$ . The model domain is discretized with  $64 \times 64$  or  $128 \times 128$  2-D variable size quadrilateral elements. The horizontal length of elements is uniformly  $1/64$  or  $1/128$ . The vertical length is  $0.7/32$  (or  $0.7/64$ ) for  $0 \leq z^* < 0.7$ , and  $0.3/32$  (or  $0.3/64$ ) for  $0.7 \leq z^* \leq 1.0$ . The shorter vertical length is used to accurately model the dynamics of the less viscous upper mantle, and it is used down to  $z^* = 0.7$  to handle subtle phase boundary deflection around  $z^* = 0.75$ . The higher resolution mesh is used for runs with  $Ra_{UM} > 4 \times 10^5$ . Time stepping is the same as by *Korenaga and Jordan* [2003a]. In addition to these runs, we also conducted some Monte Carlo experiments to test the degree of randomness inherent in this initial value problem. An example for  $Ra = 10^6$ ,  $\mu_2/\mu_1 = 30$ , and  $\Phi = -0.07$ , is shown in Figure 3 with 30 different Monte Carlo realizations for initial perturbations. It can be seen that uncertainty in breakdown time is amplified from that in onset time, and we can only aim for a more

approximate scaling law for breakdown time. Though each of the main model runs used only one realization of random perturbations, we expect that the main model runs as a whole can capture the major statistical characteristics of layering breakdown, given the wide range of model parameters we employed.

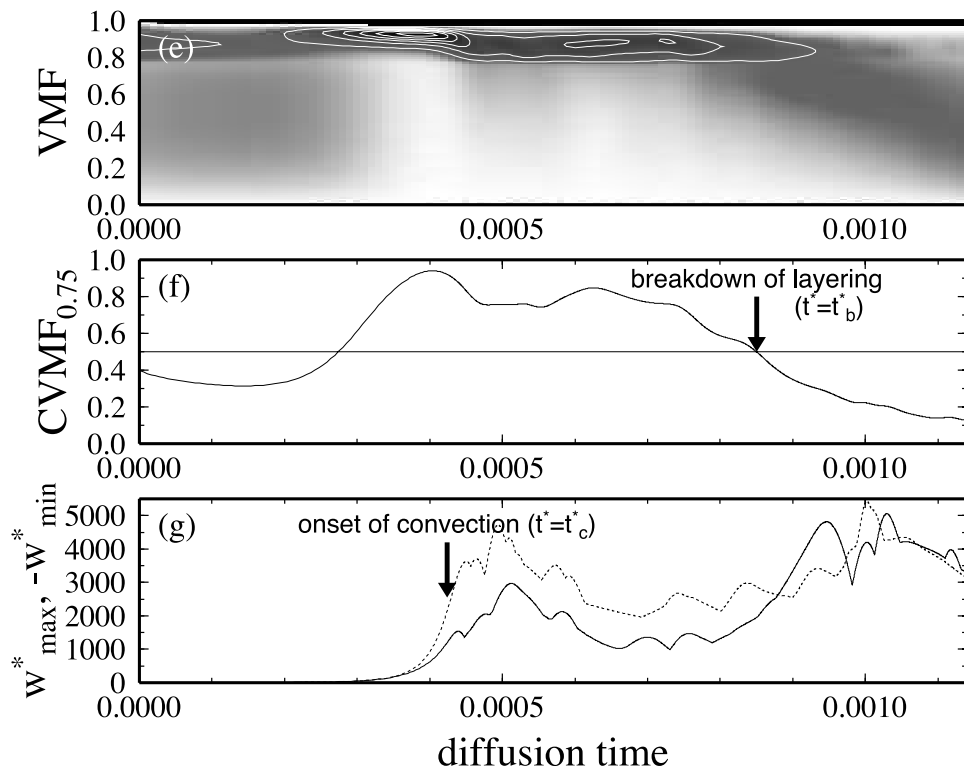
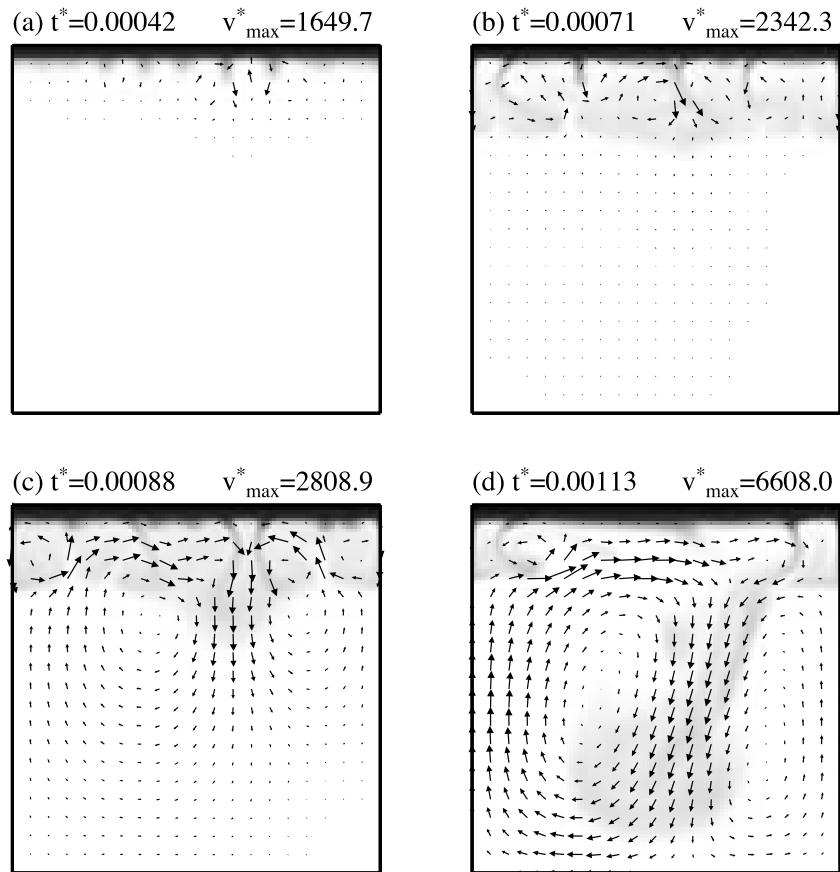
[18] An example from the main model runs is shown in Figure 4, for the case of  $Ra_2 = 10^7$ ,  $\mu_2/\mu_1 = 30$ , and  $\Phi = -0.07$ . The activation energy is set as  $92 \text{ k mol}^{-1}$  based on morphological similarity. As in the work by *Korenaga and Jordan* [2003a], the onset of convection is determined based on the deviation from the purely conducting profile. The visual inspection of snapshots indicates that the transition of convective pattern from a layered state (Figures 4a and 4b) to a whole mantle one (Figures 4c and 4d) is reasonably well captured by a vertical mass flux diagnostic (Figures 4e and 4f). The breakdown of layered convection results in a vigorous overturn (Figure 4d), like a ‘‘mantle avalanche’’ [e.g., *Tackley et al.*, 1993] but with a much smaller temperature scale.

[19] Modeling results are first examined in terms of morphological similarity. The onset time of convection (Figure 5a), the thickness of a rigid lid (Figure 5b), temperature at the base of the lid (Figure 5c), and viscosity contrast in sublithospheric convection (Figure 5d) are measured, and they are compared with theoretical predictions. The theoretical onset time,  $t_c^*$ , is based on our scaling law [*Korenaga and Jordan*, 2003a, equation (24)], in which  $Ra$  is replaced with  $Ra_2 \mu_2/\mu_1$  because the onset of convection is controlled by upper mantle viscosity. Accordingly the boundary layer timescale is redefined as

$$t_r^* \equiv \left( Ra_2 \frac{\mu_2}{\mu_1} \right)^{-\frac{2}{3}}. \quad (14)$$

As described earlier, the theoretical lid thickness is calculated as  $2 \eta_0 \sqrt{t_c^*}$ . On the basis of the conducting profile, therefore, the theoretical prediction for temperature at the lid base is given by  $T_b^* = \text{erf}(\eta_0)$ . From this predicted basal temperature, a theoretical viscosity contrast in sublithospheric convection is calculated as  $\mu^*(T_b^*)$ .

[20] A good agreement between predictions and measurements is observed in general. Some systematic misfits are also seen, which originate in the different nature of each prediction. In particular, we note that it is possible to compare directly measurements with predictions only for the onset time of convection, for which we have an explicit scaling law. A nearly perfect agreement is indeed achieved for the onset time (Figure 5a); minor deviations are consistent with the random nature of the onset time (standard deviation of  $\sim 10\%$  [*Blair and Quinn*, 1969]). For other three quantities, i.e., lid thickness, basal temperature, and viscosity contrast, comparison becomes less straightforward. The thickness of a rigid lid at the onset of convection, for example, is assumed to be calculated from the origin of available buoyancy as  $\delta_c = 2 \eta_0 \sqrt{t_c^*}$ . Though this is a reasonable approximation, it is still a mere assumption. Our actual measurement of lid thickness is based on horizontally averaged advective heat flux, following [*Jaupart and Parsons*, 1985]. There is no theoretical guarantee that this dynamically defined thickness matches the static prediction. At the onset of convection, in fact, measured



values are larger than the target thickness of 0.0345 especially for weaker temperature dependency (or lower Rayleigh number). Measured thickness, however, gradually approaches to the target value as time proceeds (Figure 5b). This agreement at later times is intriguing; the target thickness is calculated on the basis of available buoyancy, and yet it is close to measurements based on advective heat flux. Temperature at the lid base, the measurement of which is also based on advective heat flux, is systematically higher than the prediction (Figure 5c). The misfit at the onset of convection,  $t^* = t_c^*$ , is because the target thickness is rarely achieved at the onset (Figure 5b). Persistent misfit observed for later times simply originates in the convective destruction of a mobile thermal boundary layer. In other words, after the onset of convection, the theoretical prediction based on a conducting temperature profile is no longer valid.

[21] A similar explanation can be used for a viscosity contrast in convecting mantle, because both its prediction and measurement are based on the basal temperature. A large misfit is observed in Figure 5d because the temperature dependency of the Arrhenius viscosity law is super-exponential. The highest viscosity contrast achieved in the model is  $\sim 6$ . The overall trend with the parameter  $\sigma$  can be modeled as  $\sim 60\%$  of the theoretical prediction based on  $\eta_0$ . This suggests that the lid thickness may be limited by the maximum viscosity contrast that can be delaminated by convective instability, and that better theoretical predictions for  $\delta_c$  and  $T_b^*$  could be achieved by using some kind of the maximum viscosity contrast (such as dotted line in Figure 5d) instead of the origin of available buoyancy. Indeed, predictions based on the 60% viscosity contrast do seem to work quite well (dotted lines in 5b and c).

[22] The measurements of breakdown time,  $t_b^*$ , are summarized in Figure 6. As expected, layered convection lasts longer with a larger viscosity contrast and a higher phase buoyancy parameter. By least squares, we derive the following expression for the breakdown time:

$$\log\left(\frac{t_b^* - t_c^*}{t_r^*}\right) = a_0 + a_1 \Phi + a_2 \log\left(\frac{\mu_2}{\mu_1}\right) + a_3 \log Ra_{UM}, \quad (15)$$

where  $a_0 = -4.012$ ,  $a_1 = -14.510$ ,  $a_2 = 0.526$ , and  $a_3 = 0.494$ . A standard deviation for this formula is 0.33 in the logarithmic scale. This standard deviation is larger than expected from the inherent randomness of breakdown time (Figure 3), so we are not overfitting data. Convection with higher Rayleigh number tends to be characterized with shorter wavelengths, so the positive correlation between the breakdown time and the upper mantle Rayleigh number (i.e.,  $a_3 > 0$ ) is consistent with the wavelength dependency of phase change dynamics.

[23] To better understand the sensitivity of breakdown time with respect to model parameters, equation (15) may be rewritten as

$$\Delta t_b^* \equiv t_b^* - t_c^* \sim e^{-4-14.5\Phi} Ra_2^{-0.17} \left(\frac{\mu_2}{\mu_1}\right)^{0.35} \sigma^{-0.38} \left(\frac{d - \delta_c}{D}\right)^{1.5}, \quad (16)$$

where we have used equations (11) and (14) as well as the following approximation,

$$\Delta T_{UM} \sim \text{erfc}(\eta_0) \sim \sigma^{-0.75}. \quad (17)$$

The second approximation in the above works well for  $2 < \sigma < 50$  with the Arrhenius viscosity. The period of layered state after the onset of convection,  $\Delta t_b^*$ , increases with more negative  $\Phi$  and larger viscosity contrast, as already evident in Figure 6a, and decreases with greater  $Ra_2$  or  $\sigma$ . It is easy to understand the negative exponent for  $Ra_2$ ; higher  $Ra_2$  implies greater convective instability of the whole mantle system, which can lead to earlier breakdown of layered convection. Layered state also breaks down more easily with greater  $\sigma$ , because convection becomes more sluggish with stronger temperature dependency of viscosity. More sluggish convection is characterized by thermal anomalies with longer wavelengths, which can penetrate an endothermic phase boundary with less difficulty.

[24] A couple of dimensionalized examples may be informative here. The above scaling law is nondimensionalized by the whole mantle diffusion time, which is about 270 Gyr with the thermal diffusivity of  $10^{-6}$  m<sup>2</sup>/s. With  $Ra_2 = 10^8$ ,  $\Phi = -0.07$  (i.e., the Clapeyron slope of  $-2$  MPa K<sup>-1</sup> with  $\Delta\rho/\rho_0 = 0.1$  and  $\alpha = 3 \times 10^{-5}$  K<sup>-1</sup>),  $\mu_2/\mu_1 = 30$ , and  $\sigma = 20$  (equivalent to the activation energy of 300 kJ mol<sup>-1</sup>), equation (16) predicts that the breakdown of layered convection takes place  $\sim 60$  m.y. after the onset of convection. The duration of layered convection is very sensitive to the phase change parameter as its exponential dependency indicates; changing  $\Phi$  to 0 and  $-0.14$ , for example, gives the breakdown timescale of  $\sim 20$  m.y. and  $\sim 170$  m.y., respectively.

[25] Our scaling law is based on morphologically similar solutions all with the rigid lid thickness of  $\sim 100$  km. Strictly speaking, therefore, the combination of  $Ra_2$ ,  $\mu_2/\mu_1$ , and  $\sigma$  should be consistent with such specification (see Figure 2b). We expect that, however, the scaling law should be valid even for different lid thicknesses as long as the upper mantle is convecting and the lid is not too thick (i.e., less than  $d/2$ ), because of comparable finite domain effects. The lid thickness  $\delta_c$  can be estimated from  $\sigma$ ,  $Ra_2$ , and  $\mu_2/\mu_1$  as

$$\delta_c/D \sim 2\eta_0 \sqrt{t_c^*} \sim \sigma^{0.6} \left(\frac{4 Ra_c \mu_1}{\pi^2 Ra_2 \mu_2}\right)^{\frac{1}{3}}, \quad (18)$$

**Figure 4.** Example of numerical solutions for whole mantle transient cooling, with  $Ra_2 = 10^7$ ,  $\mu_2/\mu_1 = 30$ , and  $\Phi = -0.07$ . Snapshots of temperature and velocity fields are shown at (a)  $t^* = 0.00042$ , (b)  $t^* = 0.00071$ , (c)  $t^* = 0.00088$ , and (d)  $t^* = 0.00113$ . Velocity arrows are normalized by maximum velocity, which is denoted at every snapshot. Also shown are (e) vertical mass flux diagnostic (contour interval is 2.0), (f) vertical mass flux integrated from  $z^* = 0.75$  to  $z^* = 1$ , and (g) maximum upwelling (solid) and downwelling (dotted) velocities.

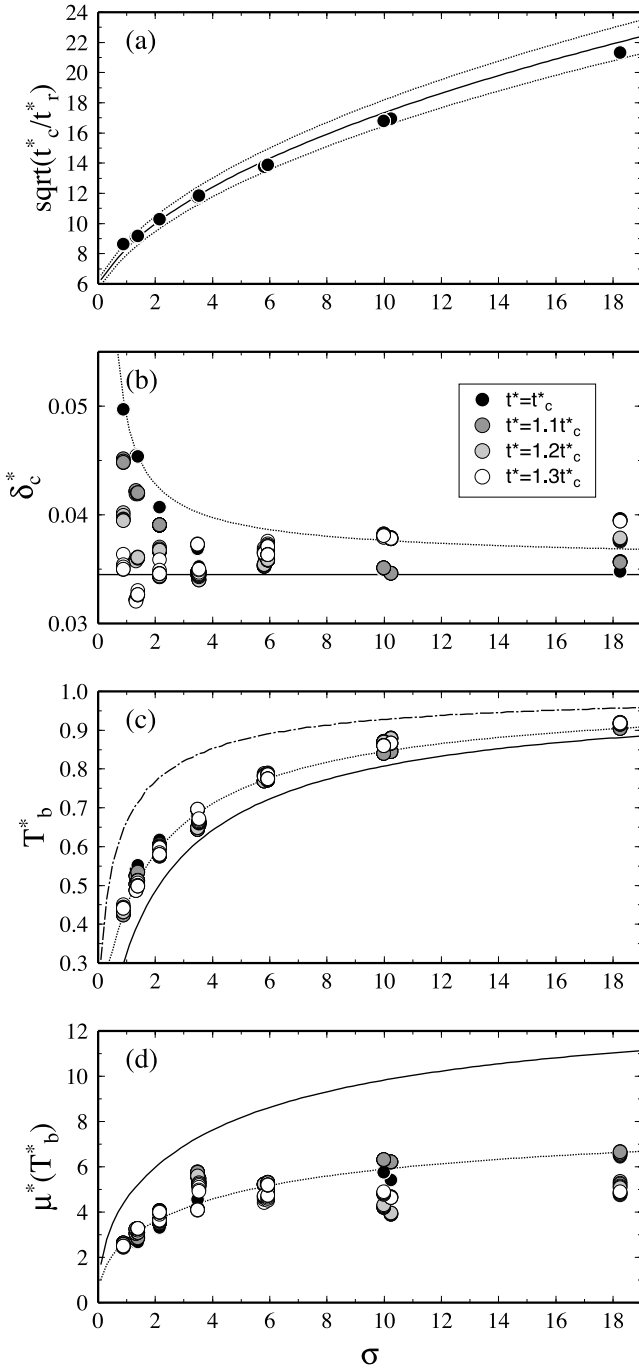


**Figure 5.** Confirmation of morphological similarity. Theoretical predictions are shown in solid lines, and measurements are shown in circles (solid circles for measurements at the onset of convection and other types of circles for subsequent measurements). All measurements are plotted as a function of the parameter  $\sigma$ . (a) Onset time. 10% standard deviation is indicated by dotted line. (b) Thickness of a rigid lid. (c) Temperature at the lid base. (d) Viscosity at the lid base. In Figures 5b–5d, theoretical predictions based on the 60% viscosity contrast are shown by dotted line. For comparison, prediction for  $T_b^*$  based on the inflection point of available buoyancy ( $\eta_i$ ) is also shown as dot-dashed line in Figure 5c.

the derivation of which involves the following approximations (under the same condition for equation (17)):

$$\eta_0 \sim 0.53\sigma^{0.25} \quad (19)$$

$$F(\sigma) \sim \sigma^{-1.05}. \quad (20)$$

Here  $F(\sigma)$  is a scaling factor used in the onset time formula [Korenaga and Jordan, 2003a].

[26] We also measured the strength of convection in terms of maximum vertical velocity,  $u_m^*$  (defined as a logarithmic average of maximum upwelling and downwelling velocities). The measured values of  $u_m^*$  are compared with predictions based on boundary layer theory [e.g., Turcotte and Schubert, 1982; Korenaga and Jordan, 2002a]:

$$u_p^* = \frac{d - \delta_c}{D} \left( \frac{Ra_2}{8} \frac{\mu_2}{\mu_1} q_s^* \right)^{\frac{1}{2}}, \quad (21)$$

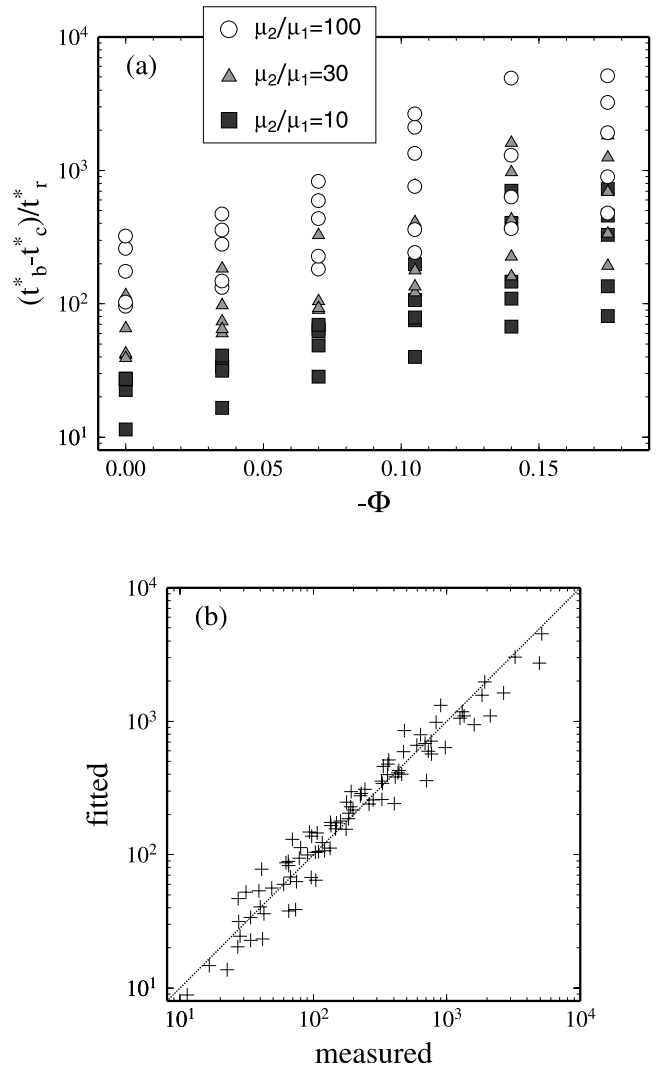


**Figure 6.** Measurements of breakdown time,  $t_b^*$ . (a)  $(t_b^* - t_c^*)/t_r^*$  as a function of phase buoyancy parameter,  $\Phi$ . Different symbols denote different viscosity contrasts. For each combination of  $\Phi$  and  $\mu_2/\mu_1$ , there are five model runs with different values of  $Ra_2$ . (b) Comparison of measured  $(t_b^* - t_c^*)/t_r^*$  with predicted values based on equation (15).



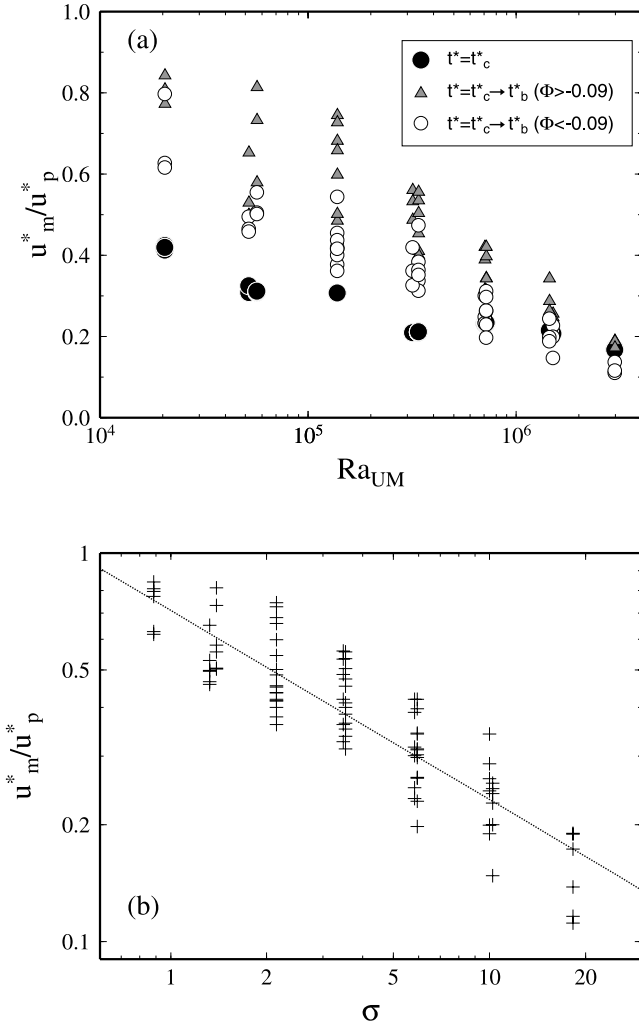


**Figure 7.** Convective velocity and boundary layer theory. The ratio  $u_m^*/u_p^*$  is plotted (a) as a function of  $Ra_{UM}$  and (b) as a function of  $\sigma$ . Dotted line in Figure 7b corresponds to equation (22).

where  $q_s^*$  is surface heat flux at the onset of convection, i.e.,  $q_s^* = 1/\sqrt{\pi t_c^*}$ . Strictly speaking, this prediction is only applicable for steady state convection, but it can serve as reference velocity, to which our measurements from transient convection can be compared. At the onset of convection,  $u_m^* \leq 0.4 u_p^*$  (Figure 7a). In terms of its temporal average for the period of layered convection,  $u_m^* \sim u_p^*$  for low  $Ra_{UM}$ , and this agreement degrades with increasing  $Ra_{UM}$ . This systematic discrepancy may be better characterized as the effect of temperature-dependent viscosity because the above theoretical prediction is based on the energetics of isoviscous convection. A scaling law for velocity is thus derived as

$$\log\left(\frac{u_m^*}{u_p^*}\right) = b_0 + b_1 \log \sigma, \quad (22)$$

where  $b_0 = -0.340$  and  $b_1 = -0.487$  (Figure 7b). Its standard deviation is around 0.21 in the logarithmic scale. Because we are dealing with temporal averages calculated

for highly transient convection with widely varying averaging periods among different runs, this large uncertainty seems to be inevitable. Compared with similar laws derived for stationary state rigid lid convection [e.g., *Solomatov and Moresi, 2000*], however, our scaling law is more relevant to sublithospheric convection beneath oceanic lithosphere, which is fundamentally transient [e.g., *Korenaga and Jordan, 2002b*]. Given that a typical lifetime of oceanic lithosphere is less than 200 m.y., we do not expect that sublithospheric convection could reach a statistically steady state.

[27] Regarding relevance to the real mantle, temperature variations associated with sublithospheric convection should also be mentioned here. Using the temperature at the base of the rigid lid,  $T_b^*$ , a total temperature variation introduced in the sublithospheric mantle can be estimated as  $1 - T_b^*$  to first order. As indicated by Figure 5c, the temperature variation gradually decreases with increasing  $\sigma$  (or increasing  $Ra_2$ ) because a mobile sublayer becomes thinner with more strongly temperature-dependent viscosity. For model runs with low Rayleigh numbers, we had to use weakly temperature-dependent viscosity to maintain morphological similarity, resulting in unrealistic temperature variations in convecting mantle (e.g.,  $\Delta T^* \sim 0.5$ ) and thus too fast cooling of the upper mantle. This unrealistic nature of sublithospheric convection, however, gradually vanishes as the Rayleigh number increases;  $\Delta T^* \sim 0.1$  for  $\sigma > 10$  (Figure 5c). In our modeling strategy based on morphological similarity, it should be understood that unrealistic low Rayleigh number runs are included intentionally to delineate dynamical differences owing to a change in the Rayleigh number.

[28] The number of convective overturns during the phase of layered convection,  $N_o$ , may be estimated as

$$N_o = \frac{(t_b^* - t_c^*)u_m^*D}{4(d - \delta_c)}, \quad (23)$$

in which one half of temporally averaged maximum vertical velocity,  $0.5 u_m^*$ , is assumed to represent average convective velocity. A scaling law is also derived for this quantity as

$$\log N_o = a_0 + a_1 \Phi + a_2 \log\left(\frac{\mu_2}{\mu_1}\right) + a_3 \log Ra_{UM}, \quad (24)$$

where  $a_0 = -3.965$ ,  $a_1 = -11.765$ ,  $a_2 = 0.414$ , and  $a_3 = 0.148$ , with a logarithmic standard deviation of 0.26. This implies that layered structure will break down after only a couple of overturns, with modest values for phase boundary buoyancy and viscosity layering.

## 5. Dynamic Regimes Beneath Evolving Lithosphere

[29] Together with our previous results [*Korenaga and Jordan, 2003a, 2003b*], we now have the following three basic scaling laws for the evolution of sublithospheric convection in oceanic mantle, i.e., (1) onset of convection, (2) stability of longitudinal rolls, and (3) breakdown of layered upper mantle convection. By combining them, we

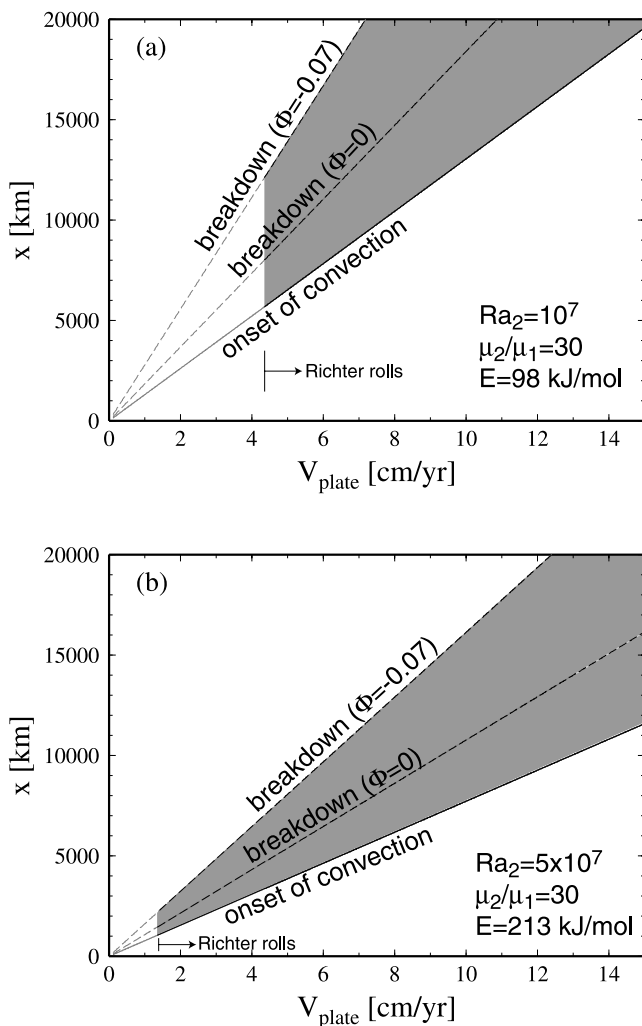


**Figure 8.** Possible convection regimes in oceanic mantle as a function of plate velocity and distance from a ridge axis. (a) The case of  $Ra_2 = 10^7$ ,  $\mu_2/\mu_1 = 30$ , and  $E = 98$  kJ mol $^{-1}$ , and (b) the case of  $Ra_2 = 5 \times 10^7$ ,  $\mu_2/\mu_1 = 30$ , and  $E = 213$  kJ mol $^{-1}$ . The value of  $E$  is chosen to have  $\delta_c = 100$  km. Dashed lines denote the location of layering breakdown for the cases of  $\Phi = 0$  and  $-0.07$ . Shading denotes where longitudinal rolls are stable in the framework of layered upper mantle convection. The upper mantle Rayleigh number is greater than  $5 \times 10^5$  in Figure 8b, for which we used  $Pe \geq \sim 300$  as the stability condition based on the experimental data of *Richter and Parsons* [1975].

can map out possible dynamic regimes expected beneath oceanic lithosphere (Figure 8). Because we do not know accurately all mantle parameters required to dimensionalize them, this exercise remains preliminary. Several simplifications made in our approach, such as a single jump in the reference viscosity profile, also precludes us from making a precise prediction for Earth’s mantle. In reality, there is probably a viscosity gradient in the upper mantle, giving rise to weak asthenosphere and more viscous transition zone. The former controls the thickness of the rigid lid while the latter affects the strength of the upper mantle convection as well as the viscosity contrast at 660 km. Such two-faced role of upper mantle viscosity could still be

modeled by equation (16), if the viscosity contrast is calculated with average upper mantle viscosity and the lid thickness  $\delta_c$  is estimated separately by asthenospheric viscosity, though this attempt may prove to be too crude.

[30] From these diagrams, nonetheless, we can learn at least what kind of a dynamic state we could expect beneath oceanic lithosphere. For a sufficiently long-lived oceanic plate, there are four possible scenarios for sublithospheric convection: (1) the classical Richter roll case (layered convection with stable longitudinal rolls for the entire life time of plate), (2) the multimodal layered case (layered convection without well-defined longitudinal rolls), (3) the Richter overturning case (whole mantle overturn with initially layered longitudinal rolls), and (4) the totally unstructured case (multimodal convection evolving from upper mantle to whole mantle scale). As seen in Figure 8, the multimodal layered case and the totally unstructured case are expected only for a limited parameter space, especially if the Rayleigh number is sufficiently high. The stability zone of Richter rolls prior to the breakdown of layered convection may even extend to slower plate motion than indicated by Figure 8, because our stability criterion is based on isoviscous convection [*Korenaga and Jordan, 2003b*]. With temperature-dependent viscosity, the roll structure may be fortified by the basal topography of the rigid lid (V. S. Solomatov, personal communication, 2003).

[31] For a fast moving plate such as the Pacific plate, the formation of Richter rolls seems to be inevitable (Figure 8), and even with moderate phase boundary buoyancy and viscosity layering, locally layered convection can be maintained for a significant fraction of plate life time (Figure 8b). We note that, however, it is not so straightforward to predict the dynamics of a 3-D system by combining scaling laws based on a 2-D system. In particular, our numerical modeling that is used to derive the breakdown scaling law does not fully capture the three dimensionality of the problem, even when longitudinal rolls are stable. Out-of-plane variations in thermal and rheological structure are the natural corollary of transient sublithospheric convection, and the dynamics associated with such variations is neglected in the 2-D modeling. It is thus of first priority to solidify our understanding of sublithospheric convection by 3-D numerical modeling (J. Korenaga and T. H. Jordan, manuscript in preparation, 2003). Preliminary dynamic regime diagrams like Figure 8 will be useful to design our modeling strategy.

## 6. Concluding Remarks

[32] For sublithospheric, “small-scale” convection in the presence of plate tectonics, we have derived several scaling laws to characterize its potential evolutionary path. Sublithospheric convection is expected to be confined to the upper mantle, at least for a while after its onset, because of a viscosity increase and an endothermic phase change expected at the base of the upper mantle. Such layered state, however, is prone to large-scale flow reorganization, because the base of the upper mantle is probably not strong enough to support thermal anomalies associated with sublithospheric convection for a sufficiently long time. The time scale for such breakdown of layered upper mantle convection to whole mantle-scale convection was studied based on a 2-D convection model that incorporates temperature- and

depth-dependent viscosity as well as phase change dynamics. For reasonable mantle values (i.e., 30-fold viscosity increase and a phase change with 10% density jump and the Clapeyron slope of  $-2 \text{ MPa K}^{-1}$ ), the breakdown time is roughly twice as long as the onset time. That is, if the onset of convection takes place beneath 50-m.y.-old seafloor, the transition to whole mantle-scale sublithospheric convection would be expected beneath 100-m.y.-old seafloor.

[33] Our study thus indicates that it is quite likely to have various kinds of sublithospheric convection beneath a sufficiently long-lived plate. This potential wealth of dynamics may be able to explain self-consistently both (1) the presence of regular Richter rolls beneath the relatively young portion of the Pacific plate (east of the Tonga-Hawaii corridor: younger than 100–120 Ma) as inferred by *Katzman et al.* [1998] and (2) the more distorted pattern of thermal anomalies beneath the older part of the Pacific plate (west of the Tonga-Hawaii corridor) as suggested by the seismic tomography of *Chen et al.* [2000].

[34] **Acknowledgments.** This work was sponsored by the U.S. National Science Foundation under grant EAR-0049044. We thank Rafi Katzman, Li Zhao, and Liangjun Chen, whose work was the primary source of inspiration for our study. We also thank Slava Solomatov and several anonymous official reviewers, whose input was helpful for improving the clarity of the manuscript.

## References

- Bercovici, D., G. Schubert, and P. J. Tackley (1993), On the penetration of the 660 km phase change by mantle downflows, *Geophys. Res. Lett.*, *20*, 2599–2602.
- Blair, L. M., and J. A. Quinn (1969), The onset of cellular convection in a fluid layer with time-dependent density gradients, *J. Fluid Mech.*, *36*, 385–400.
- Buck, W. R., and E. M. Parmentier (1986), Convection beneath young oceanic lithosphere: Implications for thermal structure and gravity, *J. Geophys. Res.*, *91*, 1961–1974.
- Butler, S., and W. R. Peltier (1997), Internal thermal boundary layer stability in phase transition modulated convection, *J. Geophys. Res.*, *102*, 2731–2749.
- Chen, L., L. Zhao, and T. H. Jordan (2000), Three-dimensional seismic structure of the mantle beneath the southwestern Pacific Ocean, *Eos Trans. AGU*, *81*(48), Fall Meet. Suppl., Abstract S62D-02.
- Christensen, U. R., and D. A. Yuen (1984), The interactions of a subducting lithospheric slab with a chemical or phase boundary, *J. Geophys. Res.*, *89*, 4389–4402.
- Christensen, U. R., and D. A. Yuen (1985), Layered convection induced by phase transitions, *J. Geophys. Res.*, *90*, 10,291–10,300.
- Davaille, A., and C. Jaupart (1994), Onset of thermal convection in fluids with temperature-dependent viscosity: Application to the oceanic mantle, *J. Geophys. Res.*, *99*, 19,853–19,866.
- Davies, G. F. (1988), Ocean bathymetry and mantle convection: 2. Small-scale flow, *J. Geophys. Res.*, *93*, 10,481–10,488.
- Dumoulin, C., M.-P. Doin, and L. Fleitout (1999), Heat transport in stagnant lid convection with temperature- and pressure-dependent Newtonian or non-Newtonian rheology, *J. Geophys. Res.*, *104*, 12,759–12,777.
- Fleitout, L., and D. A. Yuen (1984), Secondary convection and the growth of the oceanic lithosphere, *Phys. Earth Planet. Inter.*, *36*, 181–212.
- Forte, A. M., and J. X. Mitrovica (1996), New inferences of mantle viscosity from joint inversion of long-wavelength mantle convection and post-glacial rebound data, *Geophys. Res. Lett.*, *23*, 1147–1150.
- Hager, B. H., R. W. Clayton, M. A. Richards, R. P. Comer, and A. M. Dziewonski (1985), Lower mantle heterogeneity, dynamic topography and the geoid, *Nature*, *313*, 541–545.
- Honda, S., D. A. Yuen, S. Balachandar, and D. Reuteler (1993), Three-dimensional instabilities of mantle convection with multiple phase transitions, *Science*, *259*, 1308–1311.
- Howard, L. N. (1966), Convection at high Rayleigh number, in *Proceedings of the Eleventh International Congress of Applied Mechanics*, edited by H. Gortler, pp. 1109–1115, Springer-Verlag, New York.
- Ito, E., M. Akaogi, L. Topor, and A. Navrotsky (1990), Negative pressure-temperature slopes for reactions forming  $\text{MgSiO}_3$  perovskite from calorimetry, *Science*, *249*, 1275–1278.
- Jaupart, C., and B. Parsons (1985), Convective instabilities in a variable viscosity fluid cooled from above, *Phys. Earth Planet. Inter.*, *39*, 14–32.
- Jochum, K. P., A. W. Hofmann, E. Ito, H. M. Seufert, and W. M. White (1983), K, U and Th in mid-ocean ridge basalt glasses and heat production, K/U and K/Rb in the mantle, *Nature*, *306*, 431–436.
- Katzman, R., L. Zhao, and T. H. Jordan (1998), High-resolution, two-dimensional vertical tomography of the central Pacific mantle using SeS reverberations and frequency-dependent travel times, *J. Geophys. Res.*, *103*, 17,933–17,971.
- Korenaga, J., and T. H. Jordan (2002a), On the state of sublithospheric upper mantle beneath a supercontinent, *Geophys. J. Int.*, *149*, 179–189.
- Korenaga, J., and T. H. Jordan (2002b), On ‘steady-state’ heat flow and the rheology of oceanic mantle, *Geophys. Res. Lett.*, *29*(22), 2056, doi:10.1029/2002GL016085.
- Korenaga, J., and T. H. Jordan (2003a), Physics of multiscale convection in Earth’s mantle: Onset of sublithospheric convection, *J. Geophys. Res.*, *108*(B7), 2333, doi:10.1029/2002JB001760.
- Korenaga, J., and T. H. Jordan (2003b), Linear stability analysis of Richter rolls, *Geophys. Res. Lett.*, *30*(22), 2157, doi:10.1029/2003GL018337.
- Machetel, P., and P. Weber (1991), Intermittent layered convection in a model with an endothermic phase change at 670 km, *Nature*, *350*, 55–57.
- Marquart, G., H. Schmeling, G. Ito, and B. Schott (2000), Conditions for plumes to penetrate the mantle phase boundaries, *J. Geophys. Res.*, *105*, 5679–5693.
- Morris, S., and D. Canright (1984), A boundary-layer analysis of Benard convection in a fluid of strongly temperature-dependent viscosity, *Phys. Earth Planet. Inter.*, *36*, 355–373.
- Nakakuki, T., H. Sato, and H. Fujimoto (1994), Interaction of the upwelling plume with the phase and chemical boundary at the 670 km discontinuity: Effects of temperature dependent viscosity, *Earth Planet. Sci. Lett.*, *121*, 369–384.
- Parsons, B., and D. McKenzie (1978), Mantle convection and the thermal structure of the plates, *J. Geophys. Res.*, *83*, 4485–4496.
- Peltier, W. R., and L. P. Solheim (1992), Mantle phase transitions and layered chaotic convection, *Geophys. Res. Lett.*, *19*, 321–324.
- Puster, P., and T. H. Jordan (1997), How stratified is mantle convection?, *J. Geophys. Res.*, *102*, 7625–7646.
- Richter, F. M. (1973a), Convection and the large-scale circulation of the mantle, *J. Geophys. Res.*, *78*, 8735–8745.
- Richter, F. M. (1973b), Finite amplitude convection through a phase boundary, *Geophys. J. R. Astron. Soc.*, *35*, 265–276.
- Richter, F. M., and B. Parsons (1975), On the interaction of two scales of convection in the mantle, *J. Geophys. Res.*, *80*, 2529–2541.
- Schubert, G., C. Anderson, and P. Goldman (1995), Mantle plume interaction with an endothermic phase change, *J. Geophys. Res.*, *100*, 8245–8256.
- Simons, M., and B. H. Hager (1997), Localization of the gravity field and the signature of glacial rebound, *Nature*, *390*, 500–504.
- Solheim, L. P., and W. R. Peltier (1994), Avalanche effects in phase transition modulated thermal convection: A model of Earth’s mantle, *J. Geophys. Res.*, *99*, 6997–7018.
- Solomatov, V. S., and L.-N. Moresi (2000), Scaling of time-dependent stagnant lid convection: Application to small-scale convection on Earth and other terrestrial planets, *J. Geophys. Res.*, *105*, 21,795–21,817.
- Tackley, P. J. (1995), On the penetration of an endothermic phase transition by upwellings and downwellings, *J. Geophys. Res.*, *100*, 15,477–15,488.
- Tackley, P. J., D. J. Stevenson, G. A. Glatzmaier, and G. Schubert (1993), Effects of an endothermic phase transition at 670 km depth in a spherical model of convection in the Earth’s mantle, *Nature*, *361*, 699–704.
- Turcotte, D. L., and G. Schubert (1982), *Geodynamics: Applications of Continuum Physics to Geological Problems*, John Wiley, Hoboken, N. J.
- Yuen, D. A., W. R. Peltier, and G. Schubert (1981), On the existence of a second scale of convection in the upper mantle, *Geophys. J. R. Astron. Soc.*, *65*, 171–190.
- Yuen, D. A., D. M. Reuteler, S. Balachandar, V. Steinbach, A. V. Malevsky, and J. J. Smedsmo (1994), Various influences on 3-dimensional mantle convection with phase transitions, *Phys. Earth Planet. Inter.*, *86*, 185–203.
- Zhong, S., and M. Gurnis (1994), Role of plates and temperature-dependent viscosity in phase change dynamics, *J. Geophys. Res.*, *99*, 15,903–15,917.

T. H. Jordan, SCI 103, Department of Earth Sciences, University of Southern California, Los Angeles, CA 90089-0740, USA. (tjordan@usc.edu)

J. Korenaga, Department of Geology and Geophysics, P.O. Box, 208109, Yale University, New Haven, CT 06520-8109, USA. (jun.korenaga@yale.edu)